Regular Article

PHYSICAL CHEMISTRY RESEARCH
Published by the
Iranian Chemical Society
www.physchemres.org
info@physchemres.org

Phys. Chem. Res., Vol. 10, No. 4, 505-518, December 2022
DOI: 10.22036/PCR.2022.319988.2002

Activated Empty Palm Fruit Bunch for the Adsorption of Heavy Metal Ions: Kinetics and Thermodynamics

B. Chukwuemeka Ekeoma[a,*], N. Soraya Sambudi[b] and C. Obineche Ndukwe[c]

[a]*Department of Chemical Engineering, Universiti Teknologi PETRONAS, Bandar Seri Iskandar, 32610, Perak, Malaysia*
[b]*Centre of Urban Resource Sustainability (CUReS), Department of Chemical Engineering, Universiti Teknologi PETRONAS, Seri Iskandar, Perak, 32610, Malaysia*
[c]*Department of Chemical Engineering, Federal University of Technology Owerri, Imo State, 460114, Nigeria*
(Received 15 December 2021, Accepted 18 March 2022)

The efficacy of activated empty palm fruit bunch as an adsorbent for the uptake of copper, iron, and zinc heavy metal ions was investigated and the effects of temperature and contact time on adsorption capacity were studied. Samples of electroplating waste stream and waste vegetable oil were used and the optimum temperature for the adsorption process in both samples was determined to be 25 °C while the respective optimum contact times were 30 and 40 min. Linear regression analysis showed that the Langmuir isotherm model gave the best fit to the equilibrium adsorption data of the investigated heavy metal ions. Using Cu(II) adsorption from the electroplating waste and waste oil samples as a case study, the Langmuir isotherm gave the highest R^2 values of 0.9999 and 0.9998 respectively. The equilibrium adsorption capacity was determined to be 8.4 mg g^{-1} for the electroplating waste sample and 7.327 mg g^{-1} for the waste oil sample using the data for Fe(III) adsorption. The kinetics of the adsorption process was evaluated and the pseudo-second-order kinetic model provided the best description of the adsorption process in both samples according to the obtained R^2 values from linear regression analysis. Thermodynamic parameters ($\Delta G°$, $\Delta H°$, $\Delta S°$) were also calculated which together with other theoretical basis proved the adsorption mechanism in both samples to be physical. Results showed that adsorption was exothermic and spontaneous in both samples with $\Delta H°$ for the electroplating waste and waste oil samples calculated to be -1.14×10^{-2} kJ mol^{-1} and -1.68×10^{-3} kJ mol^{-1}, respectively.

Keywords: Granular materials, Pollution, Waste management & disposal

INTRODUCTION

Human health and the natural environment of the world today are largely at risk due to the excessive waste streams coming from different industrial processes. Of the various organic and inorganic contaminants released, the heavy metals have stood out as being significantly harmful bearing in mind their high toxicity, bioaccumulative nature, and non-biodegradable characteristic which make them persistent [1]. The fact that these heavy metals not only arise from anthropogenic sources (industrial activities) but also from natural/geogenic sources such as weathering of metal-bearing rocks and volcanic eruptions increases their significance in the study of environmental pollution [2]. The level of toxicity depends on the exposure route, duration of exposure, and absorbed dose [3]. Generally, heavy metals are classified as essential and non-essential with respect to the role they play in biological systems [1]. Heavy metals (Including the essential ones at high concentrations) adversely affect the environment and living species habiting such environment. They reduce soil fertility and are poisonous to both aquatic and terrestrial animals leading to their population decline [4]. This research work focused on the removal of copper, iron, and zinc which are essential metals but poisonous when present in large amounts.

*Corresponding author. E-mail: ekeomabernard@gmail.com

Excessive exposure to copper and zinc induces liver/kidney damage and also Alzheimer's disease [5]. High absorption of iron causes respiration issues for fishes and damages to cellular organelles when unbound to proteins in the body due to excessive presence [6]. Iron overloads have also been reported to be associated with increased cancer risk in living things [7].

Over the years, many industrial waste liquid treatment procedures have been employed, of which the adsorption technique has proved to be efficient, cost-effective, and reliable [8,9]. Adsorption is a surface phenomenon whereby gaseous or liquid molecules are attracted and retained by a solid or more rarely a liquid, thereby forming a film of the adsorbed molecules on the surface of the adsorbent. Very few adsorbents like zeolite occur naturally with other prominent adsorbents in use such as activated carbon, activated alumina, silica gel, and molecular sieve carbon being manufactured using inorganic and organic substances [10]. With the growing industrial need for optimization, adsorbents from low-cost natural raw materials with almost same efficiency with the more popular inorganic raw material based adsorbents are being sort for. Empty palm fruit bunch (EPFB) is a highly carbonaceous agricultural waste from palm oil processing [11] and was used in this research as a precursor to activated carbon. It is massively produced by the numerous palm oil mills around the world and in most cases is burnt to ash which in the long run constitutes environmental waste disposal problems and production of odours. The report published by Shahbandeh [12] in Statista market and consumer data website revealed that the global production of palm oil in 2020 was 72.27 million metric tons, with the leading exporters of palm oil worldwide being Indonesia, Malaysia, Thailand, Colombia, and Nigeria in a hierarchical order. The large availability of palm biomass across the globe should therefore be put to great use. The use of oil palm empty fruit bunch in the adsorptive removal of Cadmium was investigated by Rahmi *et al.* [13] and they recorded a maximum removal efficiency and adsorption capacity of 99.56% and 67.2 mg g^{-1}, respectively. The potential of EPFB to adsorb toxic hexavalent chromium was investigated by Rambabu *et al.* [14] and they observed an optimal removal efficiency of 58.02% with a dosage of 0.3 g, operating temperature of 30 °C, and initial feed concentration of 50 mg l^{-1}. Ooi *et al.* [15] also successfully showed in their research focused on urea adsorption that high adsorption capacity can be achieved using nanoporous activated carbon synthesized from oil palm biomass. Previous research works done agree that EPFB after going through the required physical and chemical modifications presents an activated carbon with the high degree of microporosity and high surface area which favours a high adsorption capacity. Thoe *et al.* [16] summarized the properties of EPFB determined from investigations made by different research groups. They presented the carbon, hydrogen, nitrogen, sulphur, oxygen, lignin, hemicellulose, cellulose, and pH percentage ranges as 40.93-68.3, 2.88-7.33, < 0.1-2.18, 0.04-0.92, 26.4-51.78, 10-34.37, 19.5-38.8, 22.2-65 and 7.20-7.80 respectively. The surface area (m^2 g^{-1}) range was also shown to be 1.48-28.4.

This research aimed at achieving both waste-to-resource conversion and environmental remediation by studying the use of activated carbon from empty palm fruit bunch for the adsorption of heavy metals. The effects of temperature and contact time as process parameters were considered. Findings from this study are industrially relevant as this research contributes to cost minimization and optimization in waste management.

METHODOLOGY

Materials Collection

The EPFB was obtained from a palm oil mill in Imo State, Nigeria. The waste stream from the electroplating process (sample A) was got from an electroplating company in Kaduna State, Nigeria while the waste vegetable oil (sample B) was obtained from a restaurant in Imo State, Nigeria.

Preparation of the Activated Carbon and Experimental Determination of its Physical Properties

The EPFB was cut into smaller size and washed with distilled water to remove external matters. The washed cut samples were allowed to dry under sunlight for 48 h to eliminate moisture before being carbonized by charring in a muffle furnace at 400 °C for 3 h after which it was allowed to cool, ground, and sieved with a 300 micrometre sized

sieve to obtain a homogeneous fine particle size. The grinding was done using a laboratory grinding mill. 100 g of the carbonized sample was then chemically activated by mixing it with 500 ml of 3 M H_2SO_4 to form a slurry which was stirred continuously for 3 h at 450 °C using a hot plate magnetic stirrer. Subsequently, the slurry was washed with distilled water to remove the excess sulphate ions in order to maintain a pH close to 7 as this is an optimal pH for maximum adsorbate removal [17]. Filtration was done to recover the residue which was dried in an oven for 6 h at 105 °C. Post-preparation of the activated carbon, its physical properties were calculated from data generated from experimental methods. To determine the particle size, the produced activated carbon was placed on top of a set of sieves arranged in an order of decreasing size of openings (increasing mesh number) and shook vigorously for 10 min using a sieve shaker. The adjacent set of sieves that retained the highest fraction of activated carbon was observed. The size of openings in these adjacent set of sieves corresponds to the particle size distribution of the activated carbon. To determine the bulk density of the activated carbon, 10 g of the activated carbon was weighed out with a balance and boiled in 100 ml distilled water for 10 min to significantly reduce the air spaces between particles after which filtration was done followed by residue drying for 6 h at 105 °C. The dried activated carbon was then weighed completely transferred into 50 ml of distilled water in a measuring cylinder. The volume of the water displaced was recorded and the bulk density was calculated by dividing the mass of the activated carbon sample by the volume of water displaced [18].

$$Bulk\ density = \frac{Mass\ of\ dried\ activated\ carbon\ sample}{Volume\ of\ water\ displaced} \quad (1)$$

The pH of the activated carbon was determined by dissolving 1 g activated carbon sample in 10 ml distilled water. The resulting mixture was stirred for 5 min to ensure proper dilution of the sample. The clear solution was filtered out and its pH was determined using a pH meter [19]. For the ash content, 1 g of the activated carbon was placed in a crucible of known mass and heated for 1 h in a pre-heated muffle furnace already at a maintained temperature at 1000 °C. Subsequently, cooling of the crucible and its content was done in a desiccator after which the crucible with its content was reweighed. The lost mass is the ash content of the activated carbon sample. The percentage ash content was calculated according to the Eq. (2) [19].

$$Ash\ content\ (\%) = \frac{Mass\ of\ ash\ (lost\ mass)}{Mass\ of\ activated\ carbon\ sample\ before\ ashing} \quad (2)$$

To determine the pore volume and porosity of the activated carbon, 1 g of the activated carbon was weighed out and transferred into a measuring cylinder in order to get the total volume of the sample. This sample was poured into a beaker containing 10 ml of distilled water and was boiled for 5 min (to displace air in the sample). The content of the beaker was filtered, dried, and weighed. The decrease in mass of the activated carbon sample divided by the density of water gave the pore volume of the activated carbon. Percentage Porosity was calculated by dividing the pore volume of the particle with the total volume of the particle and multiplying by 100 [19].

$$Pore\ volume = \frac{Mass\ of\ AC\ before\ boiling\ -\ Mass\ of\ dried\ AC\ after\ boiling}{Density\ of\ water} \quad (3)$$

$$Porosity\ (\%) = \frac{Pore\ volume}{Total\ volume} \times 100 \quad (4)$$

*AC: Activated carbon.

Physico-chemical Analysis of Samples A and B

Heavy metals, conductivity, and pH. An Atomic Absorption Spectrophotometer (AAS) (Buck Scientific 2010VGB) was used to test for concentration and absorbance of copper, iron, and zinc ions in samples A and B at the initial state and after the adsorption process under varied time and temperature. Standard solutions of copper(II), iron(III), and zinc(II) salts were prepared to calibrate the spectrophotometer. 50 ml of each salt solution was used. Distilled water was used to flush the spectrophotometer of remnants that might be contained in it from previous use and was also used for flushing after each analysis.

The test for conductivity in sample A and sample B was

carried out with a conductivity meter. The conductivity meter was calibrated and inserted into 15 ml of the sample being tested, switched on and the reading recorded. For pH, 10 ml of the sample to be tested was poured into a beaker and a pH meter was inserted into it and switched on. The pH and temperature readings were recorded when the reading became stable.

Adsorption Study

Determination of optimum temperature. The adsorption process was carried out for both samples A and B for 10 min with the temperature varied from the measured ambient temperature of 25 °C to temperatures of 30, 40, 50, 60, 70, and 80 °C. 50 ml of the sample was measured and poured into seven different beakers and heated up to their respective temperatures while noting the time it took to get to that temperature. After heating to the required temperature, 4 g of the activated carbon was poured into the solution and was stirred continuously for 10 min while the temperature was kept constant. This was followed by filtration after which the absorbance and concentration values were checked using the AAS. The percentage adsorption for each corresponding temperature was calculated using the equation below [20].

$$Percentage\,adsorption = \frac{C_0 - C_t}{C_0} \times 100 \tag{5}$$

Where C_0 is the initial concentration of adsorbate and C_t is the concentration of adsorbate at time t.

Determination of the optimum time. This was done for both samples A and B at 25 °C which was observed to be the optimum temperature. Nine beakers were used, and each beaker was filled with 4 g of the activated carbon and 50 ml of the sample. The mixtures in the respective beakers were stirred for different times of 10 min, 15 min, 20 min, 30 min, 40 min, 50 min, 60 min. 70 min and 80 min respectively. After each time interval, the mixture was filtered using a filter paper inserted into a funnel and put in a conical flask. The filtrate was analysed using an AAS where absorbance and concentration readings were taken for the reduction of heavy metals. Percentage adsorption corresponding to each contact time was calculated according to Eq. (5).

Determination of adsorption capacity and equilibrium adsorption capacity. The adsorption capacity was calculated using Eq. (6) [21].

$$Adsorption\ capacity\ (Q) = \frac{(C_0 - C_t)\,V}{M} \tag{6}$$

Where C_o and C_t represent the initial concentration and concentration at time t respectively, M is the mass of activated carbon used while V is the volume of sample A or B used.

The equilibrium adsorption capacity was determined by plotting the values of Q got from varying the contact time against time. From the graph, the time at which the Q value became constant was found. This time is the equilibrium time and the corresponding C and Q values at that point are the equilibrium concentration (C_e) and the equilibrium adsorption capacity (Q_e).

Adsorption isotherms. Langmuir, Freundlich, Temkin, and Dubinin-Radushkevich isotherms were used to study the adsorption process in order to show the amount of adsorbate adsorbed on the surface of the activated carbon as a function of its concentration at constant temperature. The four linear Isotherm equations and related equations presented below were cited from the research work of Özsin *et al.* [20]

The Langmuir isotherm is linearly expressed as:

$$\frac{C}{Q} = \frac{C}{Q_m} + \frac{1}{Q_m K_L} \tag{7}$$

Where C and Q represent the concentration and adsorption capacity at a particular time respectively. Q_m is the maximum adsorption capacity and K_L is the Langmuir adsorption constant. K_L is related to the energy of adsorption and was used in calculating the separation factor (R_L) which was used to determine the nature of the adsorption.

$$R_L = 1/(1 + K_L C_O) \tag{8}$$

$R_L > 1$ Unfavourable adsorption, $R_L = 1$ Linear adsorption, $0 < R_L < 1$ Favourable adsorption and $R_L = 0$ Irreversible adsorption.

The Freundlich isotherm is linearly expressed as:

$$\ln Q = \ln K_f + \frac{1}{n}\ln C \tag{9}$$

Where K_f is the sorption capacity and 1/n is the sorption intensity.

The Temkin isotherm is linearly expressed as:

$$Q = A\ln C + A\ln K_T \tag{10}$$

Where A is related to the heat of adsorption and K_T is the equilibrium binding constant corresponding to the maximum binding energy.

The Dubinin-Radushkevich is linearly expressed as:

$$\ln Q = -B\varepsilon^2 + \ln q_s \tag{11}$$

$$\varepsilon = RT\ln\left(1+\frac{1}{C}\right) \tag{12}$$

Where B = Dubinin-Radushkevich isotherm constant, ε = Adsorption potential, q_s = Theoretical isotherm saturation capacity, R = Universal gas constant (8.314 J mol^{-1} K^{-1}) and T = Temperature in Kelvin.

Adsorption Kinetic Models

Kinetic study was done by fitting the adsorption data obtained to the pseudo-first and second-order models and also to the intra-particle diffusion model after which the corresponding rate constants were calculated. Equations for the kinetic models used were cited from the study done by Özsin *et al.* [20]

Pseudo-first order kinetic model:

$$\log(Q_e - Q) = \log Q_e - \frac{k_1}{2.303}t \tag{13}$$

Where k_1 is the pseudo-first-order adsorption rate constant and is calculated from the slope of a plot of log(Q_e - Q) against t.

Pseudo-second order kinetic model:

$$\frac{t}{Q} = \frac{t}{Q_e} + \frac{1}{k_2 Q_e^2} \tag{14}$$

Where k_2 is the pseudo second-order adsorption rate constant. The pseudo-second-order model also served to verify the experimentally determined value of the equilibrium adsorption capacity. Q_e and k_2 were calculated from a plot of t/Q against t which gives a slope of $1/Q_e$ and an intercept of $1/k_2Q_e^2$.

Adsorption Thermodynamics

Thermodynamic study of the adsorption process was done to provide information on the associated inherent energy changes. The thermodynamic parameters include the standard Gibbs free energy of adsorption (ΔG°), standard heat of adsorption (ΔH°), standard entropy (ΔS°), and the mean free energy of adsorption (E). The thermodynamic parameters were calculated using the set of equations cited from the research work of Özsin *et al.* [20].

$$\Delta G = -RT\ln K_C = -RT\ln\left(\frac{Q_e}{C_e}\right) \tag{15}$$

However, for dimensional consistency, the standard Gibbs free energy was used with the standard equilibrium constant (K_{C^0}) equal to 1 ml g^{-1}.

$$\Delta G^\circ = -Rt\ln\left(\frac{K_C}{K_{C^0}}\right) \tag{16}$$

Where K_c = (Q_e/C_e) = equilibrium constant, R = universal gas constant and T = temperature. ΔG° for this adsorption study was calculated at a temperature of 25 °C (298.15 K) as it was the optimum temperature (operating temperature) used in this study. Values of ΔG° for T = 30 °C (303.155 K) and 40 °C (313.15 K) were also calculated to generate data to enable a plot of ΔG° against T. The slope and intercept values of this plot were used to calculate the values of ΔH° and ΔS° in accordance with the linear equation below:

$$\Delta G^\circ = \Delta H^\circ - T\Delta S^\circ \tag{17}$$

The mean free energy of adsorption (E) was calculated as follows:

$$E = \frac{1}{(2B)^{0.5}} \tag{18}$$

Where B = slope from Dubinin-Radushkevich isotherm.

RESULTS AND DISCUSSION

Characteristics of Activated Carbon from EPFB

The physical properties of the produced activated are summarized in Table 1. Particle size directly affects the flow characteristics, adsorption kinetics, and filterability of the activated carbon. The finer the particle sizes of activated carbon, the higher the access to the surface area and the faster the rate of adsorption kinetics [22]. A particle size distribution of 100-150 µm was obtained for the produced activated carbon and from the investigation done on the effect of particle size on adsorption by Müller [23], this is a good size distribution range and presents moderate to the high surface area leading to high adsorption efficiency. Low ash content of 13.2% shows the highly carbonaceous nature of EPFB and indicates that it is a good raw material for the production of an efficient activated carbon [24]. A pH close to neutral was achieved after thorough washing of the synthesized activated carbon with distilled water to remove the excess sulphate ions and this is very important regarding the effectiveness of the activated carbon. At low pH, the surface is positively charged, so the performance for adsorbing cations will be low because of the corresponding electrostatic repulsion [25]. The bulk density of the activated carbon was found to be 0.48 g cm^{-3} which is favourable with respect to adsorption potential. Most commercially used activated carbons with proven good adsorption quality have bulk densities within the range of 0.4-0.5 g cm^{-3} [26]. Porosity was calculated to be 50.6% using equation 4 after getting pore and total volumes of 0.81 and 1.6 ml respectively. A porosity of 50.6% is indicative of activated carbon with a moderate porous structure [27].

Table 1. Physical Properties of Activated Carbon Sample

Physical property	Value
Particle size (µm)	100-150
Bulk density (g cm^{-3})	0.48
pH	6.8
Ash content (%)	13.2
Pore volume (ml)	0.81
Porosity (%)	50.6

Presence of Heavy Metals

Atomic absorption spectroscopy revealed the initial concentrations of Cu, Fe, and Zn ions in samples A and B. This information is shown in Table 2.

Table 2. Initial Concentrations of Tested Heavy Metals in Sample A and Sample B (mg l^{-1})

Heavy metals	Sample A	Sample B
Cu(II)	760	630
Fe(III)	830	790
Zn(II)	710	670

Removal of Heavy Metals by Produced Activated Carbon

Effect of temperature. The relationship between percentage adsorption and temperature after contact of samples A and B with activated carbon under varied temperature conditions and steady time of 10 min is shown in Figs. 1a and 1b, respectively. From Figs. 1a and 1b, the optimum temperature (temperature at which the highest percentage adsorption occurs) is shown to be 25 °C for all three heavy metals studied in both samples A and B. It was observed that an inverse relationship exists between temperature and adsorption efficiency for the three metals in both samples. The higher the temperature, the lower the percentage adsorption. Using Cu(II) as a case study, for sample A, percentage adsorption decreased from 81.3% to 69.7% as temperature was increased from 25 °C to 80 °C. For sample B, percentage adsorption of Cu(II) decreased from 75.1% to 64.8% as temperature was increased from 25 °C to 80 °C. The decrease in percentage adsorption with the increase in temperature in both samples A and B showed that the adsorption process for both samples is exothermic and physical (physisorption) [28,29]. The decrease in adsorption percentage as the operating temperature was increased is due to the fact that the forces of attraction that exist between activated carbon and the metal ions being adsorbed in a physisorption process are weak and easily

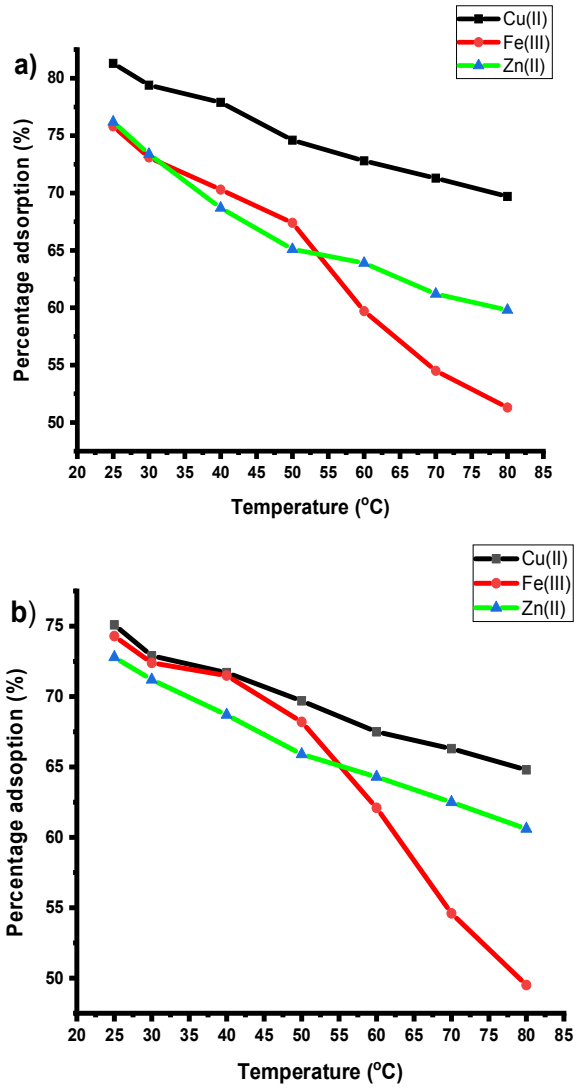

Fig. 1. Influence of temperature on percentage adsorption in (a) sample A and (b) sample B for 10 min contact time.

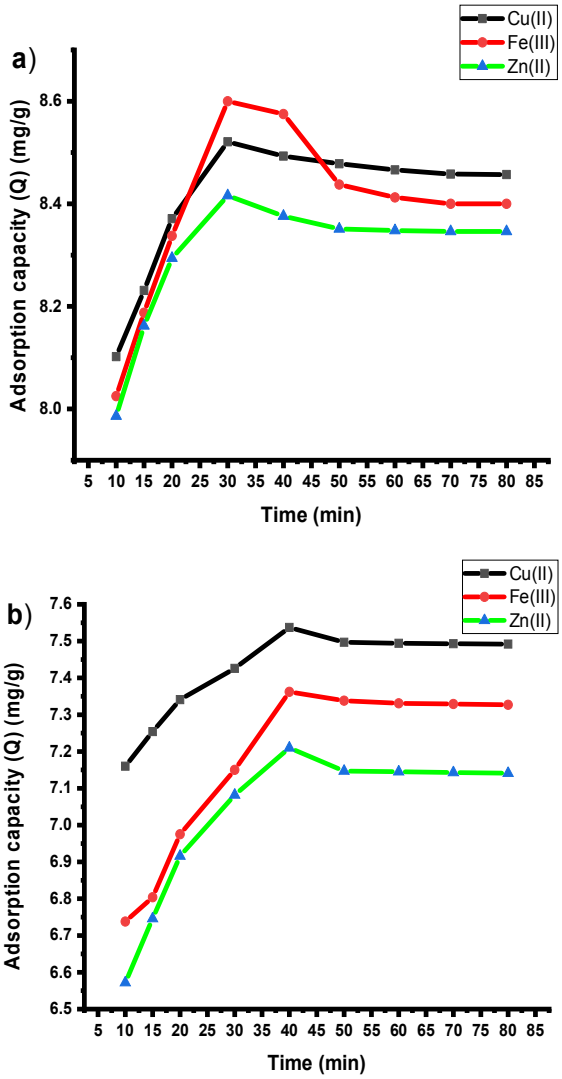

Fig. 2. Influence of contact time on adsorption capacity in (a) sample A and (b) sample B at 25 °C.

broken by the increased energy resulting from an increase in temperature. This proved the existence of the weak Van der Waals interaction force between the surface of the activated carbon and the adsorbed heavy metal ions [28].

Effect of contact time. The effect of contact time on adsorption capacity is depicted by Figs. 2a and 2b for samples A and B, respectively. From Fig. 2a, it can be seen that the adsorption capacity for sample A initially increased with time after which it started decreasing with further increase in time until equilibrium was attained. At this point, adsorption capacity remained constant despite the increase in time of contact. The optimum time (contact time at which the highest adsorption capacity occurs) was found to be 30 min for the three heavy metal ions. Using Fe(III) as a case study, the adsorption capacity of the activated carbon with respect to adsorbing Fe(III) in sample A increased initially from 8.025 mg g^{-1} to 8.6 mg g^{-1} between10 min to 30 min, dropped from 30 min to 70 min and attained a constant value of 8.4 mg g^{-1} from 70 min to 80 min. This constant value is the equilibrium adsorption capacity of the activated carbon in adsorbing Fe(III). Figure 2b shows that

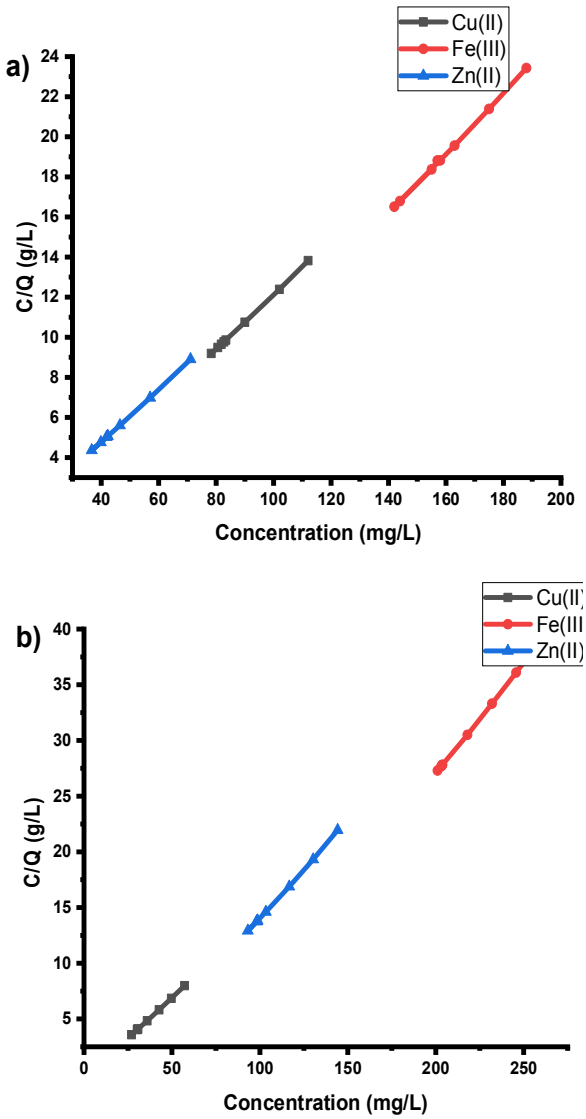

Fig. 3. Langmuir isotherm plot for (a) sample A and (b) sample B at 25 °C.

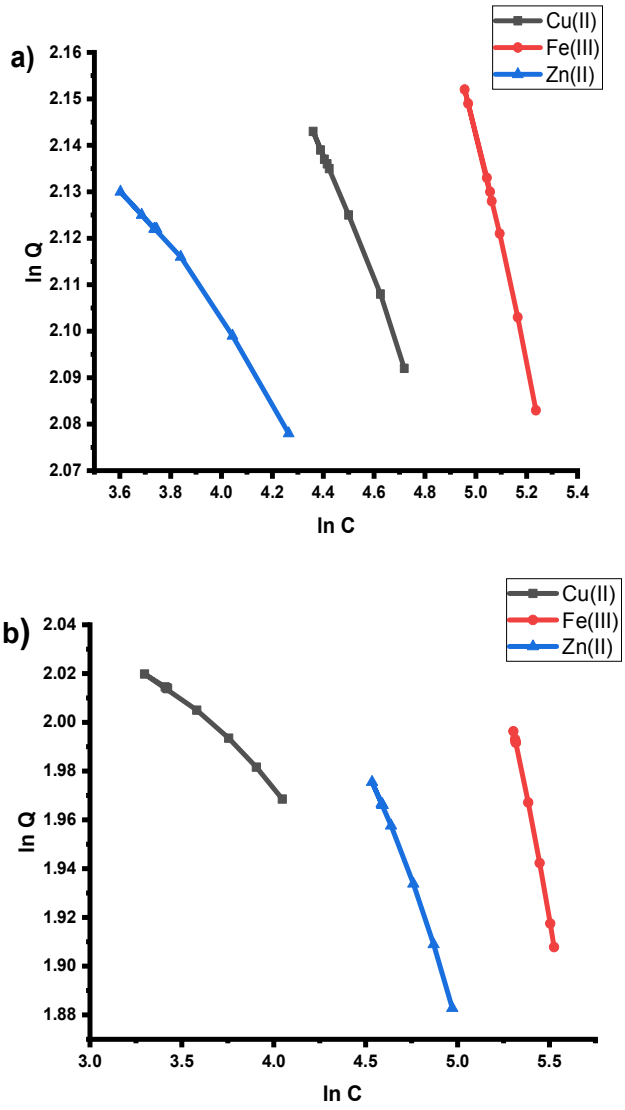

Fig. 4. Freundlich isotherm plot for (a) sample A and (b) sample B at 25 °C.

for sample B, the adsorption capacity of the activated carbon for the heavy metals under study also increased initially with time after which it dropped and later attained equilibrium. The optimum time of contact for sample B was found to be 40 min for the three heavy metals. Considering Fe(III), the adsorption capacity increased between 10 min to 40 min and started dropping from 40 minutes to 80 min with the difference in adsorption capacity becoming negligible between 70 min to 80 min to attain an equilibrium value of7.327 mg g^{-1}.

Adsorption Isotherms

The adsorption isotherms show how the adsorbed molecules distribute between the solid and liquid phase at the adsorption equilibrium state. The Langmuir, Freundlich, Temkin, and Dubinin-Radushkevich isotherm plots are shown in Fig. 3, Fig. 4, Fig. 5, and Fig. 6, respectively. Linear regression was used to determine the best fitting isotherm and the relevance of the isotherm equations were compared by evaluating their correlation coefficients. As

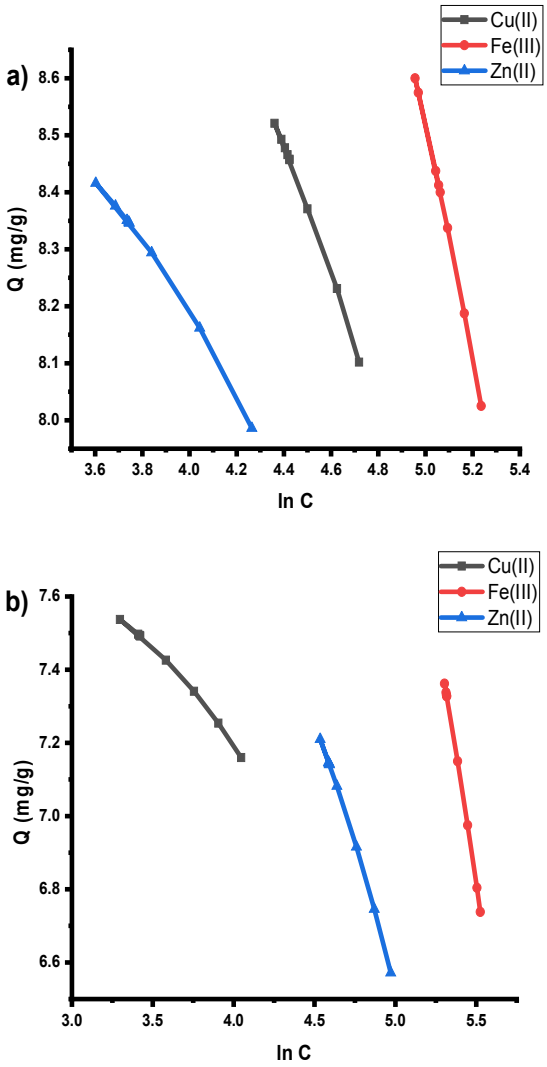

Fig. 5. Temkin isotherm plot for (a) sample A and (b) sample B at 25 °C.

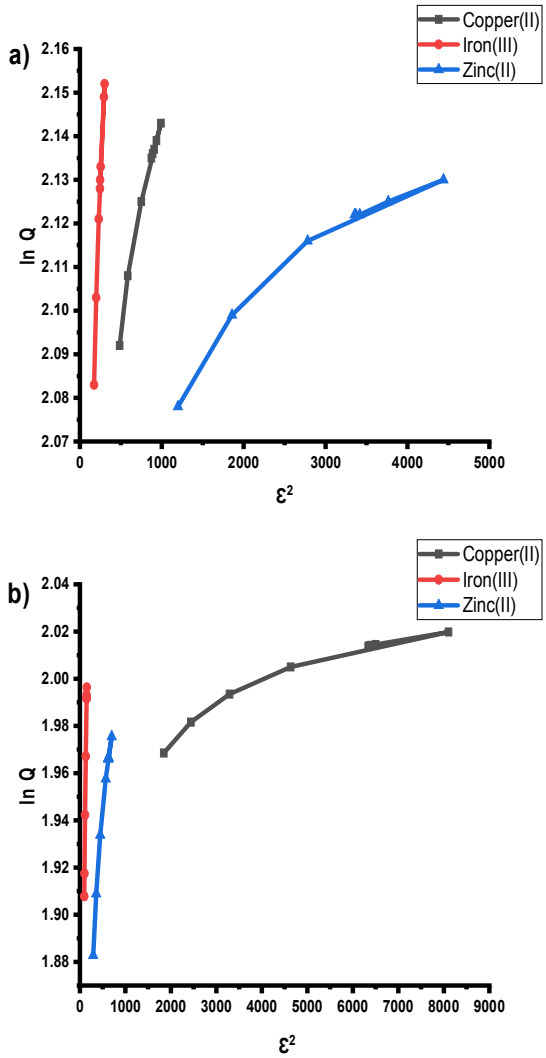

Fig. 6. Dubinin-Radushkevich isotherm plot for (a) sample A and (b) sample B at 25 °C.

shown in Table 3, the Langmuir isotherm gave the highest R^2 values for the adsorption data of all three metal ions and thus the best fit for the experimental adsorption data of Cu(II), Fe(III), and Zn(II) in sample A. For sample B, the same trend of the Langmuir isotherm is the best fit for the adsorption data of the three heavy metals was observed. Langmuir isotherm had the highest R^2 values for the adsorption data of Cu(II), Fe(III), and Zn(II) respectively. Langmuir isotherm is therefore the best representation of the adsorption process for all three heavy metals in both sample A and sample B. With Langmuir isotherm giving the best fit, the surface of the produced activated carbon can thus be said to be uniform and with a finite number of adsorption sites with each site being unable to contain a new molecule unless the already adsorbed molecule leaves. Also, no force exists between adsorbed molecules at the surface of the activated carbon [30]. The Langmuir constant (K_L) was used in calculating the separation factor R_L using Eq. (8). Using the plot for Fe(III) in Figs. 3a and 3b, R_L was calculated to be 0.0374 and 0.0733 in samples A and B

Table 3. Isotherm Constants Obtained for Heavy Metal Adsorption at 25 °C

Isotherms	Sample A			Sample B		
	Cu(II)	Fe(III)	Zn(II)	Cu(II)	Fe(III)	Zn(II)
Langmuir						
Q_m (mg g^{-1})	7.29	6.66	7.58	6.86	5.06	5.67
K_L (l mg^{-1})	0.087	0.031	0.257	0.39	0.016	0.049
R^2	0.9999	0.9993	0.9998	0.9998	0.9998	0.9995
Freundlic						
K_F ((mg g^{-1}) (l $mg^{-1})^{1/n}$)	15.7	28.94	11.23	9.45	60.2	18.82
n	7.143	4.09	12.58	14.73	2.53	4.74
R^2	0.9974	0.9969	0.9907	0.9904	0.9989	0.9961
Temkin						
A	1.165	2.042	0.655	0.5	2.80	1.45
K_T	11.68	9.17	16.49	18.4	7.94	9.5
R^2	0.9981	0.9977	0.9923	0.9918	0.9994	0.9974
Dubini-Radushkevich						
q_s (mg g^{-1})	7.75	7.38	7.89	7.11	5.79	6.21
B	1×10^{-4}	5×10^{-4}	2×10^{-5}	8×10^{-6}	1.6×10^{-3}	2×10^{-4}
R^2	0.9827	0.9773	0.9254	0.9273	0.9936	0.9739

respectively. The R_L values were thus in the range of $0 < R_L < 1$ showing that the adsorption process is favourable in both samples.

Kinetic Modelling

Figures 7a and 7b shows the pseudo-first-order and pseudo-second-order kinetic plots respectively for sample A. Figures 8a and 8b shows the pseudo-first-order and pseudo-second-order kinetic plots respectively for sample B. Linear regression was done to aid comparison and determination of the kinetic model with the best fit and the results of the regression analysis and calculated kinetic constants summarized in Table 4. The R^2 values of the pseudo-second-order kinetic model for the adsorption of the three heavy metal ions studied are higher and closer to 1 in both samples compared to the R^2 values obtained using the pseudo-first-order kinetic model. This shows that the pseudo-second-order kinetic model gives a better fit and representation of the adsorption process studied in both samples. Using the slope and intercept values of plots 7b and 8b in the pseudo-second-order model equation (Eq. (14)), the theoretical equilibrium adsorption capacity and second-order adsorption rate constant were calculated for the adsorption of all three heavy metal ions in both samples. These values are shown in Table 4 and it can be seen that the theoretical equilibrium adsorption capacities were significantly close to the experimental values.

Thermodynamic Study

The Adsorption thermodynamic parameters were evaluated to provide information on the inherent energy changes associated with the adsorption process. They were also used to determine the mechanism of adsorption (whether the adsorption is physical or chemical) and whether the adsorption process is spontaneous or not.

Table 5 shows $\Delta G°$ values evaluated at different temperatures and this data was used in making a plot of $\Delta G°$ versus time as shown in Fig. 9. From Fig. 9, $\Delta H°$ and $\Delta S°$ were calculated using the intercept and slope of the plot. The result of the calculated thermodynamic parameters is summarized in Table 6. The positive $\Delta S°$ values indicate an increase in disorderliness and randomness at the adsorption interface, leading to structural changes in both the adsorbed metal ions and EPFB activated carbon (31).

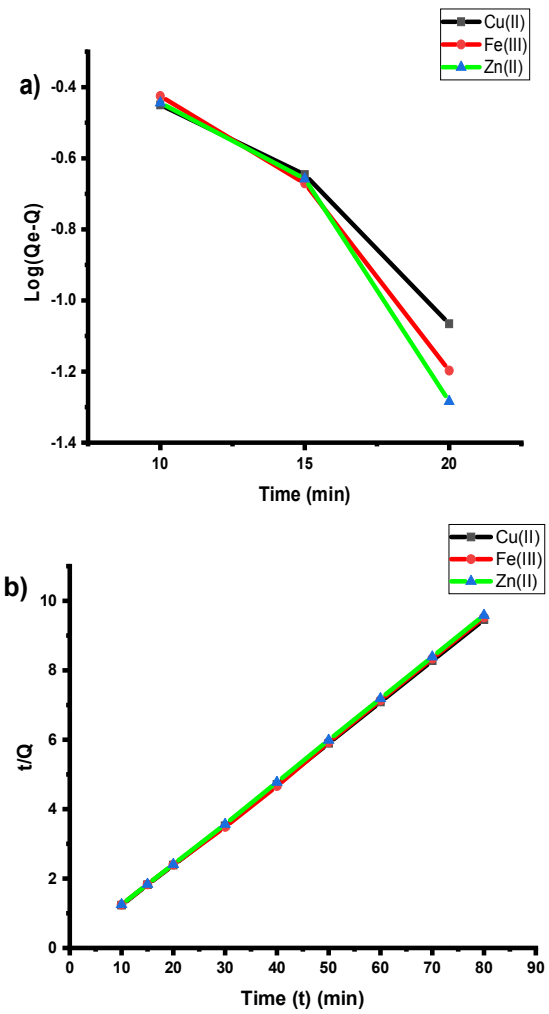

Fig. 7. (a) log(Qe - Q) against t (pseudo-first-order model) and (b) t/Q against t (pseudo-second-order model) (sample A) at 25 °C.

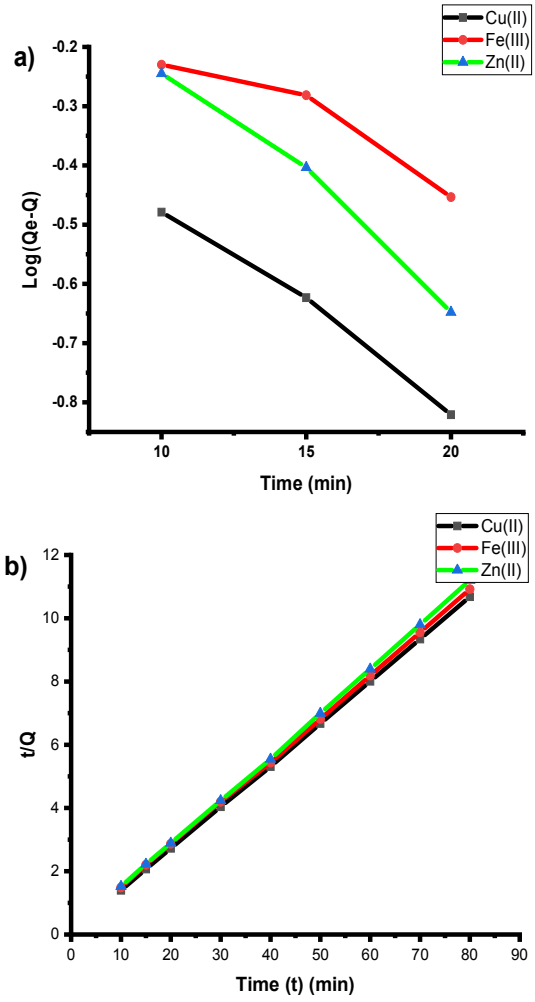

Fig. 8. (a) log(Qe - Q) against t (pseudo-first order-model) and (b) t/Q against t (pseudo-second-order model) (sample B) at 25 °C.

Table 4. Kinetic Parameters Calculated at 25 °C

Kinetic model	Sample A			Sample B		
	Cu(II)	Fe(III)	Zn(II)	Cu(II)	Fe(III)	Zn(II)
Pseudo-first order						
k_1 (min^{-1})	0.142	0.178	0.193	0.079	0.052	0.093
Q_e (mg g^{-1})	1.60	2.48	2.92	1.343	1.032	1.487
R^2	0.9579	0.9578	0.9256	0.992	0.9119	0.9851
Pseudo-second order						
k_2 (g mg^{-1} min^{-1})	0.332	1.232	0.479	0.271	0.116	0.167
Q_e (mg g^{-1})	8.525	8.439	8.382	7.553	7.463	7.241
R^2	0.9999	0.9997	0.9999	1	0.9998	0.9999

Table 5. ΔG° Value at Different Temperatures (Using Fe(II) Adsorption Data)

Temperature (K)	ΔG° (J mol^{-1})	
	Sample A	Sample B
298.15	-9,849	-8,845
303.15	-10,014	-8,993
313.15	-10,345	-9,290

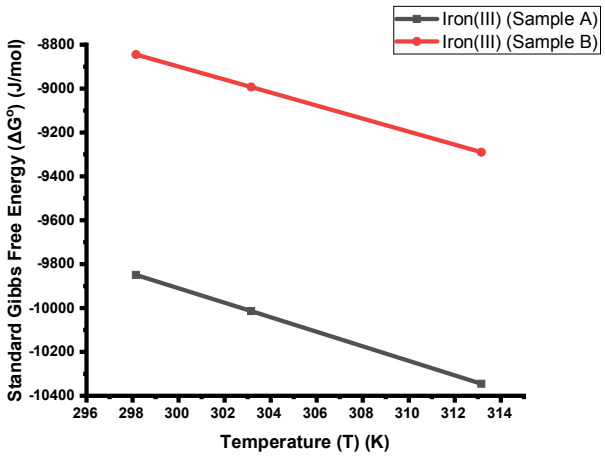

Fig. 9. Plot of ΔG° against temperature for samples A and B (using Fe adsorption data).

Table 6. Values of Thermodynamic Parameters

Thermodynamic parameter	Sample A	Sample B
Standard Gibbs free energy ΔG° (kJ mol^{-1})	-9.849	-8.845
Standard heat of adsorption ΔH° (kJ mol^{-1})	-1.14 × 10^{-2}	-1.68 × 10^{-3}
Standard entropy ΔS° (kJ mol^{-1} K^{-1})	3.3 × 10^{-2}	2.97 × 10^{-2}
Mean free energy of adsorption E (kJ mol^{-1})	3.16 × 10^{-2}	1.77 × 10^{-2}

The negative ΔH° values for adsorption in sample A and sample B (-1.14 × 10^{-2} kJ mol^{-1} and -1.68 × 10^{-3} kJ mol^{-1}, respectively) shows that the adsorption of the investigated metal ions is exothermic in both samples, and this verifies the inverse relationship that exists between adsorption capacity and temperature considering the postulates made by Mojoudi *et al.* [32]. They (Mojoudi *et al.*) showed that exothermic adsorption is a physical process (physisorption) and for such process, adsorption capacity and percentage adsorption decrease with increase in temperature and vice versa. They also inferred that the mean free energy of adsorption E is lower than 20 kJ mol^{-1} for physical adsorption and for a process to be spontaneous (self-generating and occur without external cause), the ΔG° should be negative. The adsorption process in this study is therefore exothermic in nature and a physical process. Table 6 shows the ΔG° values to be -9.849 kJ mol^{-1} and -8.845 kJ mol^{-1} in sample A and Sample B respectively. According to Mojoudi *et al.* [32], this shows that the adsorption process is spontaneous in both samples.

CONCLUSIONS

EPFB-derived activated carbon has been successfully shown to be a great adsorbent for heavy metal ions and an economic alternative for commercially available adsorbents. This research work contributes to the continuous search for cheap but effective remediation materials and also helps reduce environmental waste disposal issues associated with massively available empty palm fruit bunch. From the study carried out and results obtained, activated carbon prepared from empty palm fruit bunch, a low-cost agricultural waste has good physical properties with regards to adsorption potential and when used under the right conditions of time and temperature serves as an effective adsorbent with a good purification capacity. A temperature of 25 °C was most favourable for the adsorption process in both samples investigated, while the optimum time of contact varied with the nature of the liquid being treated. For waste stream from an electroplating process (sample A), the optimum time was 30minutes while for waste vegetable oil (sample B), the optimum time was 40 min. The adsorption process in both samples used in this research was physical, exothermic, spontaneous, and best defined by the pseudo-second-order

kinetic model and Langmuir isotherm.

REFERENCES

[1] Selvi, A.; Rajasekar, A.; Theerthagiri, J.; Ananthaselvam, A.; Sathishkumar, K.; Madhavan, J.; Rahman, P. K., Integrated remediation processes toward heavy metal removal/recovery from various environments- A review. *Front. Environ. Sci.* **2019**, *7*, 66-74, DOI: 10.3389/fenvs.2019.00066.

[2] Li, C.; Zhou, K.; Qin, W.; Tian, C.; Qi, M.; Xan, Y.; Han, W., A review on heavy metals contamination in soil: effects, sources and remediation techniques. *Soil Sediment Contam.* **2019**, *28*, 380-394, DOI: 10.1080/15320383.2019.1592108.

[3] Aprile, A.; Bellis, L., Heavy metals accumulation, toxicity and detoxification in plants. *Int. J. Mol. Sci.* **2020**, *21*, 4103-4120. DOI: 10.3390/ijms21114103.

[4] Okereafor, U.; Makhatha, M.; Mekuto, L.; Uche-Okereafor, T.; Sebola, D.; Mavumengwana, V., Toxic metal implications on agricultural soils, plants, animals, acquatic life and human health. *International. Int. J. Environ. Res. Public Health* **2020**, *17*, 2204-2221, DOI: 10.3390/ijerph17072204.

[5] Shen, X.; Chi, Y.; Xiong, K., The effect of heavy metal contamination on humans and animals in the vicinity of a zinc smelting facility. *PLoS One* **2019**, *14*, DOI: 10.1371/journal.pone.0207423.

[6] Gemaque, T. C.; Da Costa, D. P.; Pereira, L. V.; Campos, K. C., Evaluation of iron toxicity in the tropical fish Leporinus friderici. *Biomed. J. Sci. Technol. Res.* **2019**, *18*, 47-61, DOI: 10.26717/BJSTR.2019.18.00312.

[7] Wang, F.; Huanhuan, L.; Zhao, B.; Zhou, L.; Wang, S.; Luo, J.; Liu, J.; Shang, P., Iron and leukemia: new insights for future treatments. *J. Exp. Clin. Cancer Res.* **2019**, *38*, 406-419, DOI: 10.1186/s13046-019-1397-3.

[8] Burakov, A. E.; Galunin, E.V.; Burakova, I. V.; Kucherova, A. E.; Agarwal, S.; Tkachev, A. G.; Gupta, V. K., Adsorption of heavy metals on conventional and nanostructured materials for wastewater treatment purposes: A review. *Ecotoxicol. Environ. Saf.* **2018**, *148*, 702-712, DOI: 10.1016/j.ecoenv.2017.11.034.

[9] El Kassimi, A.; Regti, A.; Laamari, M. R.; El Haddad, M., Adsorptive removal of anionic dye from aqueous solutions using powdered and calcined vegetables wastes as low-cost adsorbent. *Arab J. Basic Appl. Sci.* **2018**, *25*, 93-102, DOI: 10.1080/25765299.2018.1517861.

[10] Baimenov, A.; Berillo, D. A.; Poulopoulos, S. G.; Inglezakis, V. J., A review of cryogels synthesis, characterization and applications on the removal of heavy metals from aqueous solutions. *Adv. Colloid Interface Sci.* **2020**, *276*, 545-566, DOI: 10.1016/j.cis.2019.102088.

[11] Zubaidah, S.; Hartoyo, A. P.; Sihombing, J. K.; Herliyana, E. N.; Darmawan, S.; Sari, N. R.; Prabowo, M. N.; Hermawan, I.; Maulida, I.; Solikhin, A., Oil palm empty fruit bunch valorization for activated and non-activated carbon nanoparticles and its heavy-metal-removal efficiency. Water Sci. Technol. **2021**, 83, 2652-2668, DOI: 10.2166/wst.2021.166.

[12] Shahbandeh, M., Palm oil: global production volume 2012/13-2020/21. Statista, **2021**, https://www.statista.com/statistics/613471/palm-oil-production-volume-worldwide.

[13] Rahmi, M.; Iqhrammullah, Q.; Audina, U.; Husin, H.; Fathana, H., Adsorptive removal of Cd(II) using oil palm empty fruit bunch-based charcoal/chitosan-EDTA film composite. *Sustain. Chem. Pharm.* **2021**, *21*, 478-489, DOI: 10.1016/j.scp.2021.100449.

[14] Rambabu, K.; Bharath, G.; Banat, F.; Show, P., Biosorption performance of date palm empty fruit bunch wastes for toxic hexavalent chromium removal. *Environ. Res.* **2020**, *87*, DOI: 10.1016/j.envres.2020.109694.

[15] Ooi, C. H.; Cheah, W. K.; Yeoh, F. Y., Comparative study on the urea removal by different nanoporous materials. *Adsorption* **2019**, *25*, 1169-1175, DOI: 10.1007/s10450-019-00130-5.

[16] Thoe, J. M.; Surugau, N.; Chong, H. L., Application of oil palm empty palm fruit bunch as adsorbent: A review. *Trans. Sci. Tech.* **2019**, *6*, 9-26.

[17] Achour, Y.; Khouili, M.; Abderrafia, H.; Melliani, S.; Laamari, M. R.; El Haddad, M., DFT Investigations and experimental studies for competitive and

adsorptive removal of two cationic dyes onto an eco-friendly material from Aqueous media. *Int. J. Environ. Res.* **2018**, *12*, 789-802, DOI: 10.1007/s41742-018-0131-x.

[18] Ekpete, O. A.; Marcus, A. C.; Osi, V., Preparation and characterization of activated carbon obtained from plantain (musa paradisiaca) fruit stem. *J. Chem.* **2017**, *2017*, 1-6, DOI: 10.1155/2017/8635615.

[19] Deka, K.; Medhi, B. K.; Kandali, G. G.; Pathak, K.; Das, R.; Nath, D. C.; Hazarika, P. P., Physicochemical characteristics of activated biochar derived from different sources. *Int. J. Biochem. Res.* **2018**, *22*, 1-9, DOI: 10.9734/IJBCRR/2018/42571.

[20] Özsin, G.; Kilic, M.; Ayapidin-Varol, E.; Pütün, A. E., Chemically activated carbon production from agricultural waste of chickpea and its application for heavy metal adsorption: equilibrium, kinetic, and thermodynamic studies. *Appl. Water Sci.* **2019**, *9*, DOI: 10.1007/s13201-019-0942-8.

[21] Guo, J.; Song, Y.; Ji, X.; Ji, L.; Cai, L.; Wang, Y.; Zhang, H.; Song, W., Preparation and characterization of nanoporous activated carbon derived from prawn shell and its application for removal of heavy metal ions. *Materials* **2019**, *12*, 241-263, DOI: 10.3390/ma12020241.

[22] Schulz, M.; Bünting, S.; Ernst, M., Impact of powdered activated carbon structural properties on removal of organic foulants in combined adsorption-ultrafiltration. *Water* **2017**, *9*, 580-607, DOI: 10.3390/w9080580.

[23] Müller, B. R., Preparation and characterization of K_2CO_3-doped powdered activated carbon for effective in-vitro adsorption of deoxynivalenol. *Bioresour. Technol. Rep.* **2021**, *15*, 100703-100712, DOI: 10.1016/j.biteb.2021.100703.

[24] Ravichandran, P.; Sugumaran, P.; Seshadri, S.; Basta, A. H., Optimizing the route for production of activated carbon from Casuarina equisetifolia fruit waste. *R. Soc. Open Sci.* **2018**, *5*, 171578, DOI: 10.1098%2Frsos.171578.

[25] Ullah, M.; Nazir, R.; Khan, M.; Khan, W.; Shah, M.; Afridi, S. G.; Zada, A., The effective removal of heavy metals from water by activated carbon adsorbents of Albizia lebbeck and Melia azedarach seed shells. *Soil Water Res.* **2020**, *15*, 30-37, DOI: 10.17221/212/2018-SWR.

[26] Tran, H. N.; Chao, H. P.; You, S., Activated carbons from golden shower upon different chemical activation methods: synthesis and characterization. *Adsorp. Sci. Technol.* **2017**, *36*, 95-113, DOI: 10.1177/0263617416684837.

[27] Sinha, P.; Banerjee, S.; Kar, K. K., Characteristics of activated carbon. *Handbook of Nanocomposite Supercapacitor Materials* **2020**, 125-154, DOI: 10.1007/978-3-030-43009-2_4.

[28] Marczewski, A. W.; Seczkowska, M.; Marczewska, A. D.; Blachnio, M., Adsorption equilibrium and kinetics of selected phenoxyacid pesticides on activated carbon: effect of temperature. *Adsorption* **2016**, *22*, 777-790, DOI: 10.1007/s10450-016-9774-0.

[29] El Kassimi, A.; Boutouil, A.; El Himri, M.; Lamaari, M. R.; El Haddad, M., Selective and competitive removal of three basic dyes from single, binary and ternary systems in aqueous solutions: A combined experimental and theoretical study. *J. Saudi Chem. Soc.* **2020**, *24*, 527-544, DOI: 10.1016/j.jscs.2020.05.005.

[30] Swenson, H.; Stadie, N. P., Langmuir's theory of adsorption: A centennial review. *Langmuir* **2019**, *35*, 5409-5426, DOI: 10.1021/acs.langmuir.9b00154.

[31] Achour, Y.; Bahsis, L.; Ablouh, E.; Yazid, H.; Laamari, M. R.; El Haddad, M., Insight into adsorption mechanism of Congo red dye onto bombax buonopozense bark activated-carbon using Central composite design and DFT studies. *Surf. Interfaces* **2021**, *23*, DOI: 10.1016/j.surfin.2021.100977.

[32] Mojoudi, N.; Mirghaffari, N.; Soleimani, M.; Shariatmadari, H.; Belver, C.; Bedia, J., Phenol adsorption on high microporous activated carbons prepared from oily sludge: equilibrium, kinetic and thermodynamic studies. *Sci. Rep.* **2019**, *9*, DOI: 10.1038/s41598-019-55794-4.